Chemical Physics Letters 595–596 (2014) 97–102

Contents lists available at ScienceDirect

Chemical Physics Letters

journal homepage: www.elsevier.com/locate/cplett

Free base phthalocyanine: Influence of thermal effects and dimerization on the electronic absorption spectrum

Benedito J.C. Cabral [a,b,c,*], Vinícius Wilian D. Cruzeiro [c], Kaline Coutinho [c], Sylvio Canuto [c]

[a] Grupo de Física Matemática da Universidade de Lisboa, Av. Professor Gama Pinto 2, 1649-003 Lisboa, Portugal
[b] Departamento de Química e Bioquímica, Faculdade de Ciências, Universidade de Lisboa, 1749-016 Lisboa, Portugal
[c] Instituto de Física da Universidade de São Paulo, CP 66318, 05314-970 São Paulo, SP, Brazil

ARTICLE INFO

Article history:
Received 19 December 2013
In final form 28 January 2014
Available online 3 February 2014

ABSTRACT

Theoretical results for the electronic properties of the free base phthalocyanine monomeric and dimeric species are presented. The binding energy for the most stable dimer (a parallel-displaced structure) is 12 kcal/mol. The calculations of the electronic excitation spectrum rely on the analysis of structures generated by Born–Oppenheimer Molecular Dynamics at 500 ± 4 K (monomer) and 700 ± 4 K (dimer). The results for the absorption spectrum illustrate the importance of taking into account thermal broadening and dimerization. The Q_x–Q_y band splitting is ~40 nm in reasonable agreement with the experimental value of 64 nm at T = 783 K.

1. Introduction

There is an increasing interest in the design of supramolecular structures for organic photovoltaics and artificial photosynthesis [1–5]. A particularly important class of species playing a central role in these fields are porphyrins and phthalocyanines [6,1,3,2,7]. However, for these species, some fundamental aspects such as electronic absorption, dynamics of excitonic propagation and charge transfer [8] are still not well understood [9]. One problem of interest concerns the role played by thermal effects and the associated structural distortions of the phthalocyanine skeleton on their electronic properties. Actually, the experimental absorption spectra for the metal free phthalocyanine and their complexes with several different metallic species [10] are, in many cases, for gas samples at temperatures above 500 K [10,11]. Thermal effects are therefore of fundamental importance to discuss, for example, the location of the protons in the internal cavity of the free base phthalocyanine, a subject that was related to the anomaly of the free base phtalocyanine electronic spectrum relative to metallized species [10,12]. This anomaly was characterized by a Q_x–Q_y band splitting and by broadening of the Q_x band with temperature [10]. Other issue that deserves a special attention concerns the role played by aggregation, specifically, dimer formation on the electronic properties of phthalocyanines.

Aggregation of large aromatic moieties is driven by dispersion interactions [13–16]. Therefore a correct description of these interactions is essential to determine the structures and electronic properties of porphyrins and phthalocyanines aggregates. Theoretical progress in the description of dispersion interactions has been recently accomplished by including empirical corrections for the dispersion interaction energy in density functional theory methods [17–19] which can be applied to very large supramolecular complexes [19].

Several works on the electronic properties of phthalocyanines [20,12,21,24–27,22,23] and phthalocyanine dimers [28] were reported. The present Letter, is however, dedicated to the study of the dynamics and role played by thermal effects on the electronic properties of metal free phthalocyanine. Focus is placed on the relationship between the dynamics of phtalocyanine skeleton, aggregation (dimer formation) [29,30] and the electronic absorption spectrum of free base phthalocyanine. The adopted theoretical approach is based on the sequential analysis of the electronic properties for structures generated by Born–Oppenheimer Molecular Dynamics (BOMD). The presentation is organized as follows. Initially, the adopted theoretical procedures are described. This is followed by a discussion on the properties of gas-phase optimized structures. Results relying on the sequential Born–Oppenheimer/electronic structure calculations at temperatures close to the experimental conditions are then discussed. Finally, the conclusions stress the importance of taking into account aggregation and thermal effects to investigate the electronic properties of phthalocyanines.

* Corresponding author at: Grupo de Física Matemática da Universidade de Lisboa, Av. Professor Gama Pinto 2, 1649-003 Lisboa, Portugal.
E-mail address: ben@cii.fc.ul.pt (B.J.C. Cabral).

http://dx.doi.org/10.1016/j.cplett.2014.01.047
0009-2614/

2. Computational details

The free base phthalocyanine monomer and dimers A and B (see Figure 1) were optimized with the CP2K program [31]. The hybrid Gaussian and plane-wave method GPW [32] as implemented in the QUICKSTEP module [33] was adopted. Goedecker, Teter, and Hutter (GTH) norm-conserving pseudopotentials [34] were used for representing the core electrons and only valence electrons were explicitly included in the quantum mechanical density functional theory (DFT) calculations for the geometry optimizations and BOMD. DFT calculations were carried with the Perdew–Burke–Ernzerhof (PBE) exchange–correlation functional [35] (the PBE calculations with the GTH pseudopotentials will be represented as PBE[GTH]). An empirical correction to dispersion interactions (D3) proposed by Grimme et al. [18] was added to the PBE functional for the geometry optimizations and BOMD. We adopted the GPW approach, where Kohn–Sham orbitals are expanded into atom-centered double-zeta-valence-polarization (DZVP) gaussian-type orbital functions, whereas the electron density is represented with an auxiliary plane-wave basis-set. A charge density cutoff of 280 Ry was used for the auxiliary basis-set and the self-consistent-field energy threshold for calculating the electronic density was 10^{-7} Hartree. Geometry optimizations (monomer, and dimers A and B) and BOMD (monomer and dimer-A) were carried in a cubic cell of 22 Å. Non-periodic boundary conditions with the Martyna–Tuckerman Poisson solver [36] were adopted. Binding energies of phthalocyanine dimers relying on all electron single-point energy calculations with CP2K optimized geometries are also reported. These calculations were carried out with the ORCA program [37].

BOMD was performed in the canonical ensemble with a velocity scaling thermostat [38] and target temperatures T of 500 K (monomer) and 700 K (dimer-A). In contrast with the results for gas-phase optimized structures these high values of T (500 K for the monomer and 700 K for the dimer) allows us to discuss thermal effects on the structure and electronic properties of free base phtalocyanine and the temperature for the dynamics of the dimer (700 K) is close to the experimental one (T=783 K) [10]. A timestep of 0.5 fs was used. The total time of the BOMD run was 14 ps (28,000 steps). The final average temperatures were 499 ± 4 (monomer) and 698 ± 4 K (dimer-A). A given number of configurations (equally separated in time) from the last 6 ps of the BOMD run were selected for the analysis of the structure and calculation of the electronic excitation spectra by using time dependent density functional theory (TDDFT). A long–range correction scheme (LC) proposed by Iikura et al., [39] was added to the PBE functional (LC-PBE) for TDDFT calculations. The choice of the LC-PBE functional was driven by a series of benchmarks with different functionals (see Supplementary Material). It was verified that Q_x–Q_y

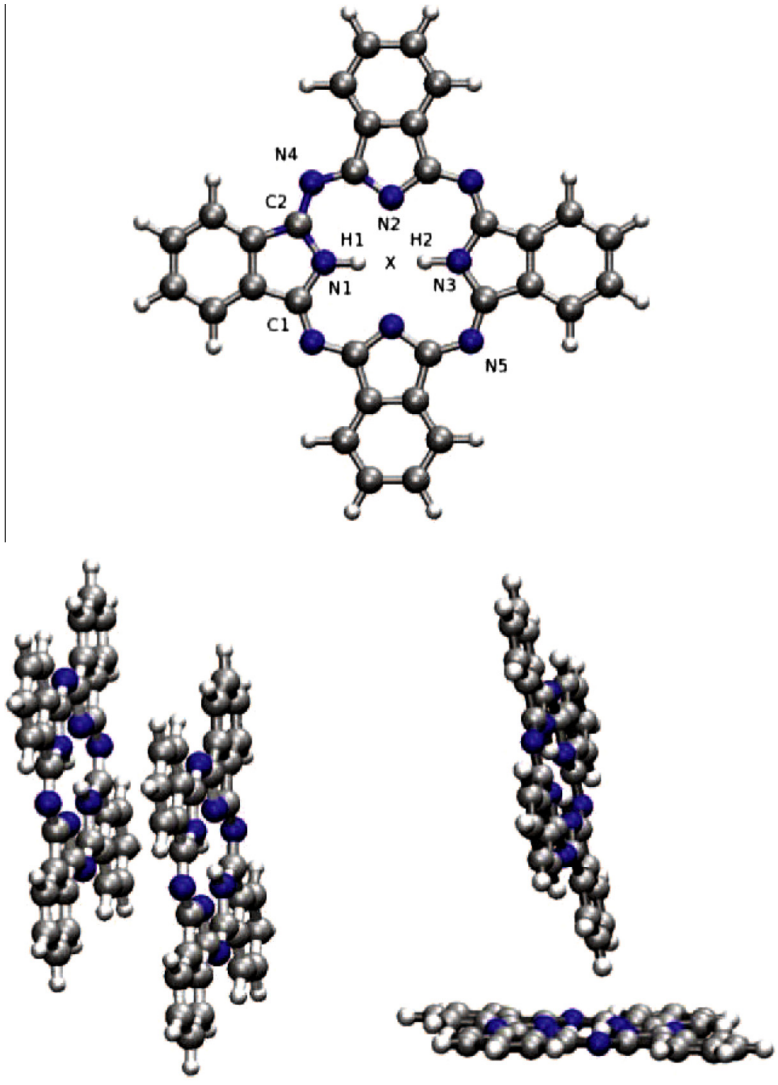

Figure 1. Optimized structures for the monomer (top) and dimers A (bottom left) and B (bottom right) of the free base phthalocyanine. For the monomer the N–H bond distance is 1.02 Å and the $N_4N_5H_2$ angle is 15.7°.

band splitting, a fingerprint of the free base phthalocyanine absorption spectrum [10], was semi-quantitatively reproduced by using the LC-PBE functional. The choice of the LC-PBE is also supported by a recent investigation on the performance of several exchange–correlation functionals for predicting excitation energies of organic molecules [40]. Excitation energies calculated with several methods are presented in Supplementary Material. Considering the size of the system and the number of configurations needed to ensure statistical convergence of the spectra (see below) excitation energies were calculated with the Sttutgart–Dresden pseudopotentials [41] and the Dunning's D95 basis-set [42,43]. TDDFT calculations were carried out with the GAUSSIAN-09 program [44].

The calculations of the spectra were carried out by using a subset of the configurations generated by BOMD. It was therefore important to investigate the convergence of the excitation energies with the number of configurations (N) included in the calculations. Figure 2 (bottom panel) shows the behaviour of the first (low energy region) and 30th (high energy region) excitations with N. These results are for the dimer-A and clearly indicate that convergence for low energy excitations are attained for $N \gtrsim 70$ configurations. Convergence for the high energy excitation is observed for $N \gtrsim 20$. Convergence of the oscillator strength f with N is also illustrated in the top panels of Figure 2 and follows the same trends observed for the excitation energies. Sequential analysis of the configurations generated by BOMD will be mainly focused on the calculations of the low energy excitation spectra. To represent the spectra, TDDFT excitation energies and oscillator strengths were convoluted by a Lorentzian distribution of 0.05 eV width.

3. Results and discussion

3.1. Gas-phase optimized structures, binding energies, and electronic spectrum

The PBE-D3[GTH]/TZVP optimized structures for the D_{2h} monomer and dimers A and B of the free base phthalocyanine are shown in Figure 1. Dimer-A is a parallel displaced structure of C_i symmetry with a distance of 4.58 Å between the two monomeric planes. The center-of-mass of each monomer will be denoted by X and the X–X distance by d(X–X), which is 5.9 Å for dimer-A. The relative displacement of the monomeric planes is 3.02 Å. Dimer-B is a perpendicular tilted structure and d(X–X) is 10.1 Å. The tilt angle, calculated as the angle between the X–X line and the monomeric plane is 12.0 degrees. The optimized structures of the free base phthalocyanine keep some similarity with optimized structures for van der Waals complexes including benzene and naphtalene [45,16]. The dimer-A parallel displaced structure is also similar to that one proposed for the π-stacked Zn–porphyrin dimer [13].

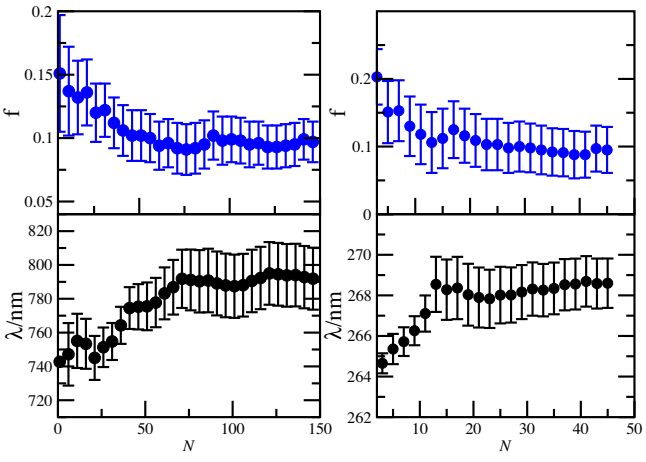

Figure 2. Convergence of the excitation energies (bottom) and oscillator strengths (top) with the number N of configurations from BOMD for dimer-A for the 1st (left) and 30th (right) excitations.

Binding energies (BEs) are reported in Table 1. The binding energy for the most stable dimer (dimer-A) is 11.3 kcal/mol at the PBE[GTH]-D3/TZVP level and no basis-set superposition error (BSSE) correction. It is in reasonable agreement with the all electron PBE-D3/TZVP calculation (12.2 kcal/mol). For dimer-A, corrections to BSSE are small with the TZVP (0.81 kcal/mol) and QZVP (0.27 kcal/mol) basis-sets. Our best estimates for the binding energies rely on all electron PBE-D3/QZVP calculations and include corrections to BSSE. They are 11.9 and 4.86 kcal/mol for dimers A and B, respectively. Therefore, our results indicate that dimer-A (a parallell displaced structure) is much more stable than dimer-B (a perpendicular structure). We are not aware of theoretical calculations for the binding energies of phthalocyanine dimers. Binding energies of van der Waals complexes were, however, the subject of several works [13,16,19]. The binding energy for a parallel displaced structure of the Zn–porphyrin dimer was reported as 11.7 ± 2.4 kcal/mol [13]. It is known that theoretical estimates of binding energies for systems stabilized by dispersion interactions are dependent on the adopted theoretical approach [16]. However, the present DFT estimates are based on the introduction of an empirical correction for the dispersion interaction [17]. In addition, recent benchmarks of dispersion interactions using DFT on large supramolecular systems [19] support the adequacy of the presently adopted approach to investigate binding energies of phthalocyanines dimers. Vibrational energy corrections to the binding energies were not taken into consideration and it is assumed that their inclusion will not change significantly our conclusions concerning the BEs and relative energies of the dimers. However, a discussion on the N–H stretching frequency in the phthalocyanine internal cavity is presented in the next section.

The absorption spectra for the optimized structures of the phthalocyanine monomer and dimers A and B are presented in Figure 3. A total number of 20 and 40 excitation energies were calculated for the optimized structures of the monomer and dimers, respectively. Data for the peak positions and oscillator strengths are also gathered in Table 2. For dimer-A the two lowest excitation energies are 697.7 nm and 665.7 nm. These transitions are forbidden (oscillator strength close to zero). The next two excitations of dimer-A (649.4 nm and 611.4 nm) are displaced to higher energies in comparison with the results for the monomer (667.5 nm and 631.8 nm). In contrast with dimer-A, the low energy excitation region ($\lambda > 500$ nm) of dimer-B shows two nearly degenerate excitations (677.6 nm; 669.8 nm and 638.7 nm; 631.9 nm) which correspond to similar localized excitations on each monomer.

Table 1
Binding energies (kcal/mol) for dimers A and B of free base phthalocyanine. Geometry optimized at the PBE[GTH]-D3/TZVP level. Binding energies without corrections to BSSE are shown in parentheses.

	Dimer A	Dimer B
PBE[GTH]-D3/TZVP[a]	(11.26)	(5.51)
PBE-D3/TZVP[b]	11.99 (12.80)	4.92 (5.25)
PBE-D3/QZVP [b]	11.94 (12.21)	4.86 (4.94)

[a] Geometry optimization with GTH [34] pseudopotentials.
[b] Single-point energy calculation with all the electrons and geometry optimized at the PBE[GTH]-D3/TZVP level. The binding energy with BSSE correction for a phthalocyanine dimer with monomers 1 and 2 was estimated as: $\Delta E = E_{12}^{12}[12] - E_1^{12}[12] - E_2^{12}[12]$, where $E_i^{12}[12]$ denotes the energy of the monomer i ($i = 1, 2$) calculated with the basis-set of the dimer (12) in the geometry of the dimer [12]. The relaxation energy contribution for each monomer $\Delta E_R = E_1^1[12] - E_1^1[1]$ was neglected.

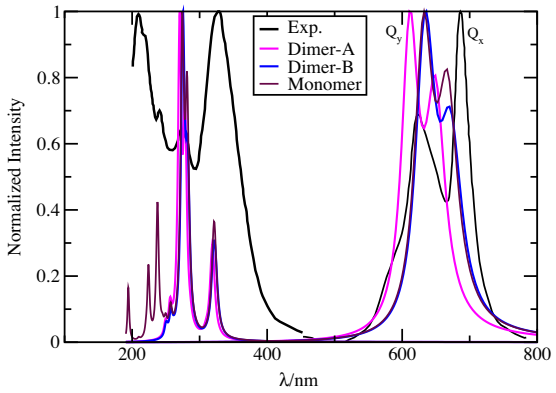

Figure 3. Excitation spectra for the optimized structures of the monomer and dimers A and B: comparison with experiment.

Table 2
Excitation energies (nm) and oscillator strengths (in parentheses) for the gas-phase phthalocyanine monomer and dimers A and B. Average values and rmsd calculated from BOMD configurations for the monomer and dimer-A are shown in italics.

Monomer	Dimer-A [a]	Dimer-B	Exp.[b]
667.5 (0.41)	649.4 (0.66)	677.6 (0.21); 669.8 (0.47)	686.0 (Q_x)
696 ± 10	*674 ± 10*		
631.7 (0.55)	611.4 (0.89)	638.7 (0.37)); 631.9 (0.77)	622.5 (Q_y)
656 ± 10	*633 ± 10*		
321.5 (0.48)	318.9 (0.67)	323.8 (0.34); 320.8 (0.58)	340.0 (B)
	278.4 (1.38)	283.4 (0.43); 281.6 (0.87)	
281.6 (0.89)	270.8 (0.95);	275.9 (1.18); 274.6 (1.49)	
274.4 (1.19)	270.2 (1.21)		280; 270 (N)
257.0 (0.08)	256.2 (0.16)	257.6 (0.11)	
237.6 (0.54)			240.0 (L)
224.2 (0.29)			220; 210 (C)

[a] The two lowest excitation energies of the gas-phase optimized structure of dimer-A (C_i symmetry) are 697.7 nm and 665.7 nm. These transitions are forbidden by symmetry.
[b] Experimental values from Edwards and Gouterman [10].

Moreover, these excitation energies are quite similar to those calculated for the isolated monomer.

In comparison with the data for the optimized structures the experimental spectra is characterized by an intense peak near 686 nm (Q_x) and by the extension of the absorption region into the low energy region above 700 nm. Other difference concerns the Q_x–Q_y splitting that is ~38 nm for dimers A and B, whereas the experimental value is ~64 nm. A good agreement between theoretical predictions and experiment for the peak positions associated with the different high energy bands is also observed.

It should be expected that inclusion of thermal effects improve the theoretical results in comparison with experiment. However, considering the significant difference between the binding energies of dimers A and B (7.0 kcal/mol), Born–Oppenheimer Molecular Dynamics were only carried out for the monomer (500 ± 4 K) and dimer-A (700 ± 4 K).

3.2. Thermal effects on the electronic absorption

The role played by structural distortions of the free base phthalocyanine skeleton induced by thermal effects on the electronic properties is of fundamental importance to understand the electronic absorption spectra of these species [10,12]. Some specific features characterizing the electronic spectra of free base phthalocyanines are a strong dependence of the Q_x–Q_y splitting on the environment as well as the anomalous broadening of the Q_y band with temperature [10]. In addition, porphyrins [46] and phthalocyanines [47] exhibit a great flexibility and deviations from planarity. It should be expected that these effects are even more important at high temperatures such as the ones where the electronic absorption spectra were measured [10] thus stressing the role played by thermal effects on the electronic properties of phatalocyanines. To investigate the relationship between structural distortions of the free base phthalocyanine skeleton and their influence on the electronic properties we first defined a set of geometric parameters. Then we followed their time evolution accordingly to the Born–Oppenheimer dynamics. By adopting thresholds for these geometric parameters we can investigate the electronic spectra for a subset of configurations corresponding to specific structural distortions.

To discuss the relationship between the Q_x–Q_y splitting and the internal H atoms position in the phthalocyanine central cavity we defined the angles NNH between two outer N atoms of the macrocycle and one hydrogen atom (this angle is defined by the N4N5H2 or N5N4H1 atoms of Figure 1). Figure 4 illustrates the time evolution of NNH predicted by the BOMD of the phthalocyanine monomer. When the two NNH angles are less than 10° the structure of the internal cavity of the phthalocyanine monomer keeps some similarity with the bridge configuration proposed by Schaffer and Gouterman [12] (it should be observed that only $\lesssim$2% of the total BOMD configurations satisfy this criterion). In a bridge configuration, it is assumed that the each proton (H_1, H_2) is shared by two neighbor N nuclei of the central cavity [10,12]. In agreement with Schaffer and Gouterman [12] the present results indicate that distortions of the internal cavity leading to structures similar to a bridge configuration effectively contribute to increase the Q_x–Q_y splitting. This is illustrated in Figure 5, where we compare the spectrum for the NNH threshold value with the full average spectrum for the monomer without no geometric constraints (BOMD) and also with the experimental data [10]. The inset panel of Figure 5 shows the dependence of the Q_x-Q_y splitting on the NNH angle. The black squares represent the averages for a set of NNH values in a 0.5° interval. Circles are the maxima and minima values in the same interval. These results indicate a correlation between the splitting and the proton positions. Moreover, it appears that when NNH is $\lesssim$8.5° the Q_x–Q_y splitting is around 120 nm and for larger NNH the splitting is around 70 nm. Although the Q_x–Q_y splitting is increased for nearly bridged configurations, these configurations are present in small number and do not contribute in a significant way to determine the average spectrum of free base phthalocyanine. In addition, Q_x for these configurations is strongly red-shifted relative to the average spectrum and experimental data. Based on the present results it seems more reasonable to assume that the observed Q_x–Q_y splitting is mainly determined by a complex set of structural distortions induced by thermal effects.

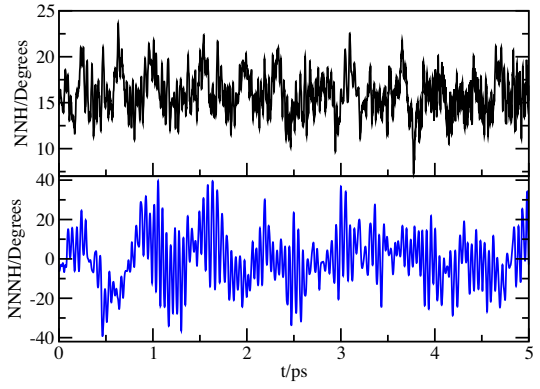

Figure 4. Time evolution of NNNH dihedral angle and NNH angle (see Figure 1) for the phthalocyanine monomer.

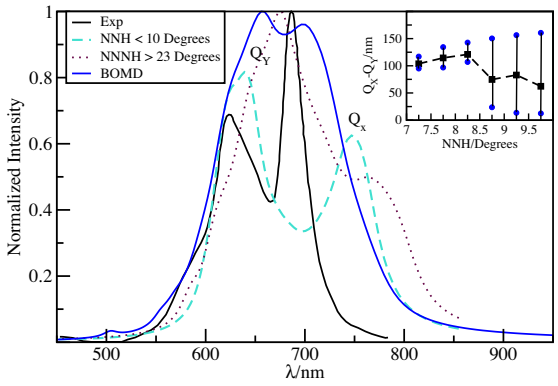

Figure 5. Influence of structural distortions on the low-energy absorption spectrum of free base phthalocyanine monomer. The inset panel illustrates the dependence of the Q_x–Q_y splitting on the NNH angle (see Figure 1).

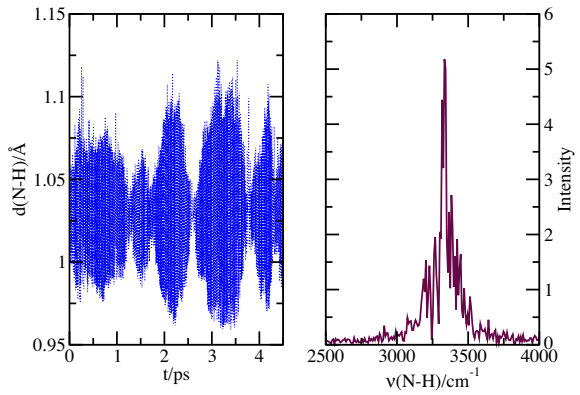

Figure 6. Time evolution of the NH bond in the central cavity (left) and frequency distribution (right) in the phthalocyanine monomer.

Deviations of the H atoms in the internal cavity from the NNN plane can be discussed by defining a dihedral NNNH angle involving two pyrroles and one aza group (this angle is defined by the N1N2N3H2 or N3N2N1H1 atoms in Figure 1). The time evolution of NNNH is shown in Figure 4 (bottom panel). We adopted the convention that significant deviations from planarity (NNNH$\sim$ 0) take place when at least one of the NNNH angles fulfills the condition abs (NNNH) > 23°. The excitation spectrum for the subset of configurations satisfying this criterion is also shown in Figure 5. These configurations contribute to reinforce an absorption peak at $\sim$680 nm. In contrast with the results for the full average spectrum, the absorption peak at $\sim$640 nm is not observed and a shoulder in the low energy region close to 750 nm is now present. Therefore, deviations of NNNH from planarity in the internal cavity of the free base phthalocyanine contribute to enhance electronic absorption at lower energies.

The time evolution of the N–H bond [d(N–H)(t)] in the internal cavity of the phthalocyanine dimer-A is illustrated in Figure 6 (left panel). The average value is 1.03 ± 0.03 Å, which can be compared with the N–H bond distance observed for the gas-phase optimized structure (1.02 Å). The right panel shows the distribution of the ν(N—H) stretching frequency that was calculated as the Fourier transform of the average velocity autocorrelation function defined as $C_{AA}(t) = < A(t)A(t_i)/A(t_i)A(t_i) >$ where $A = \frac{dx}{dt}$, t_i a time origin, and x = d(N–H). A similar procedure was recently applied to calculate the vibrational frequencies of chlorophyll-c_2 in liquid methanol [48]. This distribution shows a peak near 3300 cm^{-1}, which is the value observed for the N–H stretching frequency in different systems [49].

The structural dynamics of the phthalocyanine dimer will reflect thermal effects as well as the dispersion interactions between the monomers. The time evolution of d(X–X), the distance between the nomomers center-of-mass X, is represented in Figure 7 for a 4 ps window. These distances are in the 4.5–5.5 Å range and their distribution is associated with significant distortions of the phthalocyanine skeleton. Deviations of the phtalocyanine fragments involving the pyrrole group from the planar situation observed in the monomeric optimized structure can be estimated through the introduction of a dihedral angle (CCH-X) between the CCH plane of pyrrole and the H–X vector (C1C2H1 atoms of Figure 1 and the coordinate X). When CCH-X = ±180° for one specific pyrrole fragment, an orientation similar to the planar situation can be assumed. The time evolution of this angle is also shown in Figure 7 (bottom panel) and the results show deviations of up to $\sim$60° from the planar situation. Actually, different criteria can be defined to discuss the distortions of the phthalocyanine skeleton relative to the gas-phase optimized structure and the qualitative nature of the present analysis should be stressed.

The low-energy electronic excitation spectra for the monomer and dimer-A of phthalocyanine calculated by using a selected set of 140 configurations generated by BOMD is shown in Figure 8, where they are compared with the spectra for the optimized structures (monomer and dimer) and with experiment. Average values calculated by using BOMD configurations are also gathered in Table 2. Comparison between the results for the monomer (at T = 500 ± 4 K) and dimer (at T = 700 ± 4 K) shows a good agreement. The theoretical Q_x–Q_y splitting for both the monomer and dimer is $\sim$40 ± 14 nm, which is $\sim$24 nm below the experimental value (63.5 nm) [10]. For both the monomer and dimer, thermal effects lead to a shift to lower energies and to a significant broadening of the spectra. It should be noticed that structural distortions induced by thermal effects may contribute to broad of the low energy band of dimer-A. The two lowest excitation energies of the optimized gas-phase dimer-A are forbidden by symmetry (see Table 2). However, they become allowed for the structures generated by BOMD.

In general, a good agreement with experiment is observed for the results relying on averages over BOMD configurations. In addition, our results suggest that the main features characterizing the low energy range of the electronic absorption spectrum of free base phthalocyanine may be interpreted by assuming the presence in the vapour phase of dimeric species stabilized by dispersion interactions. The influence of dimers in the absorption spectra of phthalocyanines was discussed by Dhami et al. [30]. Some

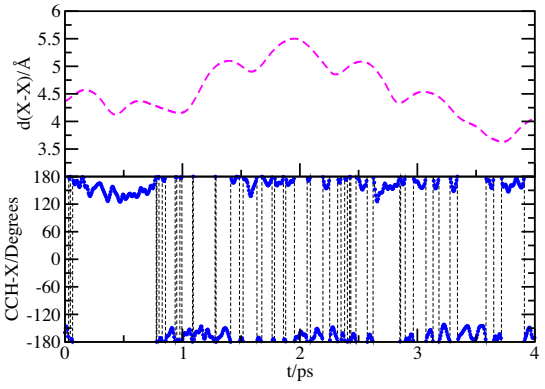

Figure 7. Time evolution of the distance between the phthalocyanine center-of-mass for dimer-A (top); time evolution of the CCH-X dihedral angle for the monomer in dimer-A (see $C_1C_2H_1$-X of Figure 1).

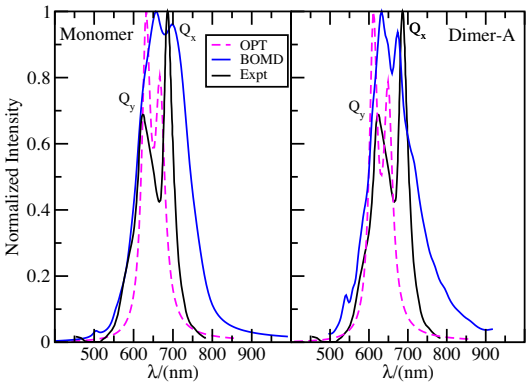

Figure 8. Low energy electronic absorption spectra for the monomer and dimer-A. Comparison with BOMD, optimized structures and experimental data.

particular features associated with dimerization are the broadening of the Q_y band and the presence a new band at the red edge of the spectrum. Our results are in keeping with these experimental findings [30].

4. Conclusions

The role played by thermal effects and dimerization on the electronic properties of free base phthalocyanine was investigated through a sequential BOMD/TDDFT approach. Our results for the binding energies of phthalocyanine dimers, mainly for the parallel displaced dimer-A, bound by 12 kcal/mol, indicate that this species could be present even at the high temperature (776 K) at which the experimental absorption spectrum was measured [10]. This conclusion is supported by the good agreement between the theoretical excitation spectrum for dimer-A and the experimental data. Thermal effects lead to important distortions of the phthalocyanine skeleton at high temperatures. The distortions are characterized by deviations from the planarity characterizing the gas-phase optimized structures. The theoretical spectra of free base phthalocyanine, for both the monomer and dimer-A are significantly broadened in the low energy region in comparison with the experimental data [10].

In agreement with previous investigations on the relationship between the proton's position in the internal cavity of phthalocyanine and the Q-band splitting, it was verified that structures similar to the bridged structures proposed by Schaefer and Gouterman [12] lead to a significant Q_x–Q_y splitting. However, these structures are present only in a small fraction of the total BOMD configurations. Consequently, our results suggest that the Q-band splitting in free base phthalocyanine is enhanced by thermal effects and it is actually determined by a complex set of structural distortions.

Acknowledgements

Partially supported by FCT (Portugal), CNPq, CAPES, FAPESP, INCT-FCx and nBioNet (Brazil). BJCC gratefully acknowledges support from the Universidade de São Paulo through a research grant.

Appendix A. Supplementary data

Supplementary data associated with this article can be found, in the online version, at http://dx.doi.org/10.1016/j.cplett.2014.01.047.

References

[1] M.G. Walter, A.B. Rudine, C.C. Wamser, J. Porphyrins Phtalocya. 14 (2010) 759.
[2] F. Ito et al., J. Phys. Chem. A 110 (2006) 12734.
[3] T. Inabe, H. Tajima, Chem. Rev. 104 (2004) 553.
[4] A. Uetomo, M. Kozaki, S. Suzuki, K.-I. Yamanaka, O. Ito, K. Okada, J. Am. Chem. Soc. 133 (2011) 13276.
[5] J.G. Woller, J.K. Hannestad, B. Albinsson, J. Am. Chem. Soc. 135 (2013) 2759.
[6] J.R. Darwent, P. Douglas, A. Harriman, G. Porter, M.C. Richoux, Chem. Rev. 44 (1982) 83.
[7] A. Takeda, T. Oku, A. Suzuki, Y. Yamasaki, J. Mod. Phys. 2 (2011) 966.
[8] K. Kilså, J. Kajanus, A.N. Macpherson, J. Mårtensson, B. Albinsson, J. Am. Chem. Soc. 123 (2001) 3069.
[9] Y. Shirota, H. Kageyama, Chem. Rev. 107 (2007) 953.
[10] L. Edwards, M. Gouterman, J. Mol. Spectrosc. 33 (1970) 292.
[11] L. Edwards, D.H. Dolphin, M. Gouterman, A.D. Adler, J. Mol. Spectrosc. 38 (1971) 16.
[12] A.M. Schaffer, M. Gouterman, Theoret. Chim. Acta 25 (1972) 62.
[13] C.A. Hunter, J.K.M. Sanders, J. Am. Chem. Soc. 112 (1990) 5525.
[14] K.S. Kim, P. Tarakeshwar, J.Y. Lee, Chem. Rev. 100 (2000) 4145.
[15] K. Müller-Dethlefs, P. Hobza, Chem. Rev. 100 (2000) 143.
[16] Y. Jung, M. Head-Gordon, Phys. Chem. Chem. Phys. 8 (2006) 2831.
[17] S. Grimme, J. Comput. Chem. 27 (2006) 1787.
[18] S. Grimme, J. Antony, S. Ehrlich, J. Chem. Phys. 132 (2010) 154104.
[19] T. Risthaus, S. Grimme, J. Chem. Theory Comput. 9 (2013) 1580.
[20] N.S. Hush, I.S. Woolsey, Mol. Phys. 21 (1971) 465.
[21] E. Orti, J.L. Bredas, C. Clarisse, J. Chem. Phys. 92 (1990) 1228.
[22] P. Toman, S. Nespurek, K. Yakushi, J. Porphyr. Phtalocya. 6 (2002) 556.
[23] M.G. Vivas, L. de Boni, L. Gaffo, C.R. Mendonça, Dyes Pigments 101 (2014) 338.
[24] K. Toyota, J.-Y. Hasegawa, H. Nakatsuji, J. Phys. Chem. A 101 (1997) 446.
[25] D.P. Piet, D. Danovich, H. Zuilhof, E.J.R. Sudhölter, J. Chem. Soc. Perkin Trans. 2 (1999) 1653.
[26] T.-T. Lu, M. Xiang, H.-L. Wang, T.-J. He, D.-M. Chen, J. Mol. Struct. (Theochem.) 860 (2008) 141.
[27] R. Fukuda, M. Ehara, H. Nakatsuji, J. Chem. Phys. 133 (2010) 144316.
[28] M.M. Mikolajczyk, R. Zalesny, Z. Czyznikowska, P. Toman, J. Leszczynski, W. Bartkowiak, J. Mol. Model. 17 (2011) 2143.
[29] D. Phillips, S. Dhami, R. Ostler, Z. Petrasek, Prog. React. Kinet. Mec. 28 (2003) 299.
[30] S. Dhami, A.J. de Mello, G. Rumble, S.M. Bishop, D. Philips, A. Beeby, Photochem. Photobio. 61 (1995) 341.
[31] http://cp2k.berlios.de, 2011.
[32] G. Lippert, J. Hutter, M. Parrinello, Mol. Phys. 92 (1997) 477.
[33] J. VandeVondele, M. Krack, F. Mohemed, M. Parrinello, T. Chassaing, J. Hutter, Comput. Phys. Commun. 167 (2005) 103.
[34] S. Goedecker, M. Teter, J. Hutter, Phys. Rev. B 54 (1996) 1703.
[35] J. Perdew, K. Burke, M. Ernzerhof, Phys. Rev. Lett. 77 (1996) 3865.
[36] G.J. Martyna, M.E. Tuckerman, J. Chem. Phys. 110 (1999) 2810.
[37] F. Neese, ORCA – An ab initio, Density Functional and Semiempirical Program Package, Version 2.9.1, University of Bonn, 2012.
[38] G. Bussi, D. Donadio, M. Parrinello, J. Chem. Phys. 126 (2007) 014101.
[39] H. Iikura, T. Tsuneda, T. Yanai, K. Hirao, J. Chem. Phys. 115 (2001) 3540.
[40] D. Jacquemin, V. Wathelet, E.A. Perpete, C. Adamo, J. Chem. Theory Comput. 5 (2009) 2420.
[41] M. Dolg, U. Wedig, H. Stoll, H. Preuss, J. Chem. Phys. 86 (1987) 866.
[42] T.H. Dunning Jr., P.J. Hay, in: H.F. Schaefer III (Ed.), Modern Theoretical Chemistry, vol. 3, Plenum, New York, 1976, p. 1.
[43] T.H. Dunning Jr., J. Chem. Phys. 90 (1989) 1007.
[44] M.J. Frisch et al., Gaussian 09, Revision A.1, Gaussian Inc, Wallingford, CT, 2009.
[45] M. Pitoňak, P. Neogrady, J. Řezáč, P. Jurečka, M. Urban, P. Hobza, J. Chem. Theory Comput. 4 (2008) 1829.
[46] T.A. Hamor, W.S. Caughey, J.L. Hoard, J. Am. Chem. Soc. 87 (1965) 2305.
[47] C.J. Brown, J. Chem. Soc. 2488 (1968) 2494.
[48] B.J.C. Cabral, K. Coutinho, S. Canuto, J. Chem. Phys. 138 (2013) 225102.
[49] N.G. Mirkin, S. Krimm, J. Phys. Chem. A 108 (2004) 5438.